Energy and Buildings 70 (2014) 303–317

Contents lists available at ScienceDirect

Energy and Buildings

journal homepage: www.elsevier.com/locate/enbuild

Setting up and validating a complex model for a simple homogeneous wall

I. Naveros [a,d,*], P. Bacher [b], D.P. Ruiz [c], M.J. Jiménez [a], H. Madsen [b]

[a] Energy Efficiency in Buildings R&D Unit, CIEMAT, Madrid E-28040, Spain
[b] Informatics, Technical University of Denmark, Richard Pedersen Plads, Building 305, 2800 Lyngby, Denmark
[c] Department of Applied Physics, University of Granada, Av. Severo Ochoa s/n, E-18071 Granada, Spain
[d] CETHIL UMR5008, INSA-Lyon, 9 rue de la physique, F-69621 Villeurbanne, France

ARTICLE INFO

Article history:
Received 15 February 2013
Received in revised form 11 October 2013
Accepted 25 November 2013

Keywords:
Building energy
Thermal parameters
Outdoor testing
System identification
Grey-box modelling
Stochastic differential equations

ABSTRACT

The present paper describes modelling of the thermal dynamics of a real wall tested in dynamic outdoor weather conditions, to identify all the parameters needed for its characterisation. Specifically, the *U* value, absorptance and effective heat capacity are estimated for the wall using grey-box modelling based on statistical methods and known physical dynamic energy balance equations, related to the heat flux density through a simple and homogeneous wall. The experimental test was carried out in a hot-temperature climate for nine months. This study aims at proposing a dynamic method improving the regression averages method for estimation of parameters which describe the thermal behaviour of the wall. Solar irradiance and long-wave radiation balance terms are added in the heat balance equation besides modelling of wind speed effect to achieve a complete description of the relevant phenomena which affect the thermal dynamics of the wall. The method is applied using different frequency data samples looking for the best to study this wall. The *U* value obtained characterising the wall is consistent with the one given by the regression averages method.

1. Introduction

There is a growing need in our society to evaluate and quantify thermal properties of the buildings and their components, to save energy and to develop better ways to characterise them. The aim is to increase comfort conditions, reduce the energy consumption and enable buildings to become interactive components in an energy system increasingly based on renewable energy production.

In a previous study a linear regression method based on averages was used to evaluate thermal properties of the same simple opaque and homogeneous wall [1]. The wall is part of a test cell, and it is tested under real weather conditions [2–4]. This method can be applied to buildings and buildings components. Its main drawback is that it requires long test periods depending on the test component and weather conditions, and in some cases may become too much time consuming or leading to unaffordable long test campaigns. Thus, previous work gave a reference regarding the *U* value estimates that can be used as additional validation criteria, and regarding accuracy, length of test, needed variables, etc., to evaluate the improvements achieved when another method is used.

This paper applies techniques based on modelling the dynamics of the system which are also able to describe non-linear effects. Grey box modelling using stochastic differential equations (SDEs) [5], is applied for estimation of *U* value, and it is also used to estimate absorptance and effective heat capacity, which were not able to be estimated when averages were used to characterise thermal performance of the wall [1]. Parameters obtained with the SDE models based on energy balance equations are employed for identifying these physical parameters [6].

Different experiments applying this modelling approach have been studied. From the thermal characterisation of building components using outdoors test cells [7], over the modelling of building integrated photovoltaic modules [8,9], and to the analysis of full size buildings [10].

Dynamic modelling in the present study [11], considers a different experiment and SDEs regarding previous works using data for a significantly longer test period to have a better description [6,7]. Furthermore, it considers a more detailed description for surface effects allowing the capability to take into account these effects in this analysis approach, giving a very valuable background for further studies on building systems.

* Corresponding author. Tel.: +34 678821237; fax: +34 950365015.
E-mail addresses: ibaname@correo.ugr.es, iban.naveros-mesa@insa-lyon.fr (I. Naveros).

0378-7788/$ – see front matter © 2013 Elsevier B.V. All rights reserved.
http://dx.doi.org/10.1016/j.enbuild.2013.11.076

Nomenclature

Measured quantities

T_e	outdoor air ambient temperature (K)
T_i	test room indoor air ambient temperature (K)
T_{se}	external surface temperature (K)
Q_i	heat flux density through the building component (W/m^2)
G_v	global vertical solar irradiance (W/m^2)
G_{lw}	vertical long wave irradiance (W/m^2)
w	wind speed on the wall (m/s)

Non-measured quantities

T_{sky}	sky temperature (K)
T_{ground}	ground temperature (K)
T_{sg}	surroundings temperature (K)

Parameters

U	total heat transfer coefficient of the wall (W/m^2 K)
g	solar energy transmittance
$C_{1,2}$	effective heat capacities of part of the test component per unit surface (W min/m^2 K)
C	effective heat capacity of the test component per unit of surface (J/K)
α, ϵ	wall absorptance and emittance
$U_{1,2,3}$	heat transfer coefficients of part of the wall (W/m^2 K)
h_{se}, h_{si}	external and internal surface heat transfer coefficient (W/m^2 K)
h_{ce}, h_{re}	external surface convective and radiative heat transfer coefficient (W/m^2 K)
$h_{r,ws}$, $h_{r,wg}$	external surface radiative heat transfer coefficient wall-sky, and wall-ground (W/m^2 K)
$h_{r,wsg}$	external surface radiative heat transfer coefficient wall-surroundings (W/m^2 K)

Constants

F_{ws}, F_{wg}	view factors wall-sky and wall-ground
F_{wsg}	view factor wall-surroundings
σ	Stefan–Boltzmann constant (W/m^2 K^4)

State variables

T, $T_{1,2}$	inside wall temperatures (K)

The text is organised as follows: in Section 2 the test component is described. In Section 3 the experiment set up is presented. Data used for the analysis are presented and discussed in Section 4. In Section 5 the methodology is presented. Finally, the results are outlined and discussed in Section 6 and the conclusions are drawn in Section 7.

2. Test component description

The data used in this paper stems from a test of a simple lightweight, opaque and homogeneous wall [12].

This wall is made of ceramic bricks which size is 32 cm × 16 cm × 11.5 cm, joined using sand and concrete mortar, Fig. 1. Exterior is plastered with mortar, 2 cm thick. Interior is gypsum plastered 1.5 cm thick. The wall total thickness is 15 cm made of 2 cm mortar, 11.5 cm brick and 1.5 cm gypsum.

The interior surface of the wall is 276 cm height by 298 cm width.

Fig. 1. Exterior view of the wall tested.

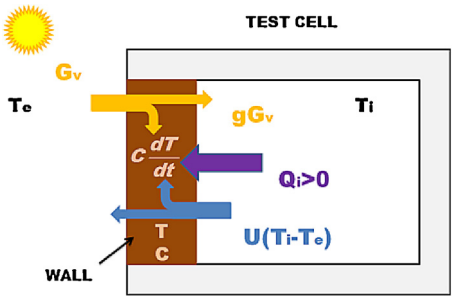

Fig. 2. Test cell scheme.

3. Experiment set up

3.1. Boundary conditions

This wall was tested in a test cell, Fig. 2, at the LECE laboratory at Plataforma Solar de Almeria,[1] in the South East of Spain (37.1° N, 2.4° W). The weather at this test location is dry and extremely hot in summer and cold in winter. The temperature difference varies considerably between day and night. Daily global vertical solar irradiation is significantly higher in winter, 22 MJ/m^2, than in summer, 12 MJ/m^2, for sunny days.[2] The sky is usually very clear.

The test was carried out under outdoor weather conditions. Set point for indoor air temperature is about 18 °C in summer and 40 °C in winter. A ventilator was used to avoid indoor air temperature stratification.

3.2. Measurements

This section describes the measurement equipment and relevant information regarding the measurement accuracy [7].

The following list summarizes the used measurement transducers and sensors, Fig. 3:

- Air temperature (T_e, T_i[°C]): Platinum thermoresistance, PT100, 1/10 DIN, directly measured using a four-wire connection, with a solar radiation shield and ventilated for outdoor measurements. Accuracy 0.1 °C.
- Surface temperature (T_{se}[°C]): Analogous sensors and connections as those used for air temperature, in this case embedded in the corresponding surface. Accuracy 0.1 °C.

[1] http://www.psa.es/webeng/instalaciones/lece.php#lece.
[2] Source: PSA-LECE Laboratory.

Fig. 3. View of several measurement instruments.

- Heat flux density (Q_i [W/m^2]): Sensor model HFP01 manufactured by Hukseflux, accuracy of sensitivity coefficient 5%, voltage measured directly using a differential connection.
- Vertical global solar irradiance (G_v [W/m^2]): Pyranometer, model CM11 manufactured by Kipp and Zonen, secondary standard according to ISO 9060:1990, voltage directly measured using a differential connection. Accuracy 3%.
- Vertical long wave radiation on the surface of the test component (G_{lw} [W/m^2]): Pyranometer, model CGR4 manufactured by Kipp and Zonen, voltage directly measured using a differential connection. Accuracy 3%.
- Wind speed (w [m/s]): Sensor model WindSonic manufactured by Gill Instruments Ltd. Accuracy 2%.

A data acquisition system, Fig. 4, with the following characteristics has been implemented: 16-bit A/D resolution, range of measurements fitting sensor output, modules distributed to minimize wiring, based in Compact Field Point modules manufactured by National Instruments. Particularly the following list summarizes the used modules:

- cFP-RTD-124: Four-wire RTD and resistance inputs. Range −200 °C to 850 °C used for measurement of temperature.
- cFP-RTD-125: Differential thermocouple or millivolt inputs. Range −20 mV to 80 mV used for measurement of global and long wave radiation and heat flux density.
- cFP-RTD-111: Milliamp input. Range 4–20 mA used for measurement of wind speed.

Twisted pairs and grounded shield are employed to reduce noise and avoiding perturbations from wiring.

4. Data

The data analysed stem from a testing period from 5th of March 2010 to 11th of October 2010, Table 1. Data are read and recorded every minute, the conditions are different throughout the testing period. Two differentiated data period are shown in detail in Fig. 5 (series 5 and 15).

Two different periods can be clearly distinguished. The first one, till the mid of June, is characterised by a relatively large positive difference between indoor and outdoor air temperatures, and also

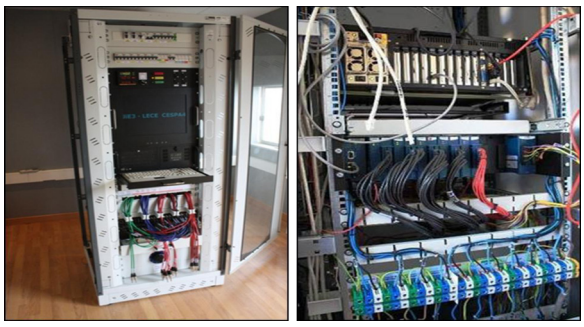

Fig. 4. View of data acquisition system (left). Wiring and connections (right).

Table 1
Date of data set analysed.

Series	Date
01	05/03/2010–14/03/2010
02	15/03/2010–24/03/2010
03	25/03/2010–03/04/2010
04	04/04/2010–13/04/2010
05	14/04/2010–23/04/2010
06	24/04/2010–03/05/2010
07	04/05/2010–13/05/2010
08	20/05/2010–29/05/2010
09	30/05/2010–08/06/2010
10	09/06/2010–18/06/2010
11	23/06/2010–02/07/2010
12	03/07/2010–12/07/2010
13	13/07/2010–22/07/2010
14	23/07/2010–01/08/2010
15	02/08/2010–11/08/2010
16	12/08/2010–21/08/2010
17	22/08/2010–31/08/2010
18	01/09/2010–10/09/2010
19	11/09/2010–20/09/2010
20	21/09/2010–30/09/2010
21	01/10/2010–10/10/2010

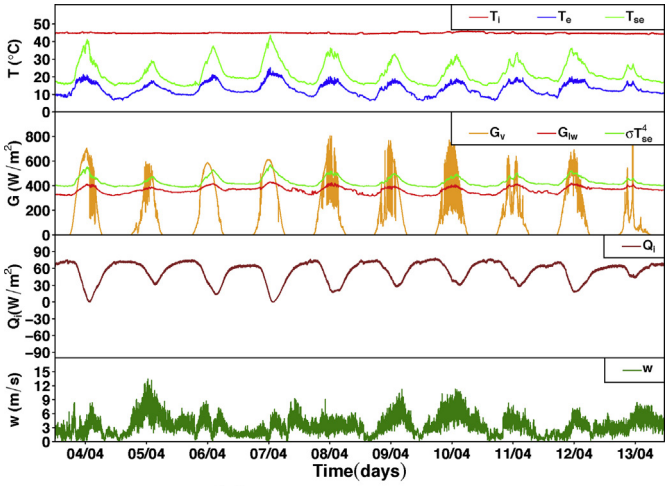

(a) *Serie 5(4-13th April).*

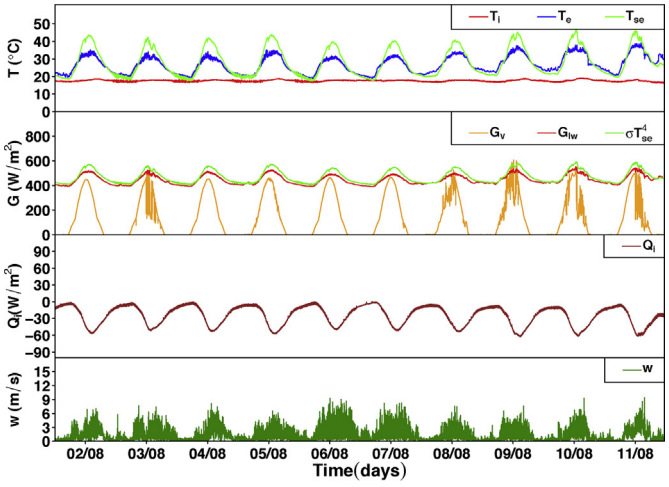

(b) *Serie 15(2-11th August).*

Fig. 5. Measured data.

by large levels of global solar radiation measured on the external surface of the wall, Fig. 5(a). The second period is characterised by a relatively small and negative difference between indoor and outdoor air temperatures, and also by lower levels of global solar radiation measured on the external surface of the wall, Fig. 5(b).

The absolute value of the heat flux density, which is mainly driven by these two effects, ranges in similar values in both periods. In the first period, when thermal energy is leaving the room, the two effects are strong and opposite. In the second period the indoor temperature level is changed and thermal energy is entering the room. However, each of these main driving effects are adding but weak in the second period, and as consequence this period is more vulnerable to uncertainties, which causes difficulties in the identification process, mainly in the first part of this second period when these effects present the lowest values.

5. Data analysis

5.1. Energy transfer

According to [13], the steady state energy balance equation which describes heat flux through a homogeneous wall is

$$Q = U(T_i - T_e) \tag{1}$$

where it is assumed that all heat flux through wall is only a consequence of difference between indoor and outdoor air ambient temperatures, T_i, T_e (°C), respectively, Q (W/m^2) is heat flux density and U (W/m^2 K) is the total heat transfer coefficient.

This equation can be used to obtain the U value from a test under dynamic conditions, replacing the steady state measurements of Q, T_i and T_e by the corresponding averages over certain test interval, provided that the conditions established in [13] are accomplished.

Nonetheless, it is known that other physical phenomena can affect the heat flux. Thus, the energy balance equation may need to include more of those variables to obtain a better description for heat flux through the wall [6].

The main variable which is necessary to include in Eq. (1) in the study of the wall is global vertical solar irradiance, G_v (W/m^2). If long wave radiation balance, B_{lw} (W/m^2), is also added between wall and its surroundings, taking into account outdoor air ambient and surroundings temperatures respectively [14], energy balance equation becomes:

$$Q = U(T_i - T_e) - gG_v + bB_{lw} \tag{2}$$

where g is the solar energy transmittance and b is, by analogy, a long wave energy transmittance.

In order to detail solar energy transmittance, g, and long wave energy transmittance, b, another way to write this energy balance equation is considering the sol–air temperature [15], T_{sa} (°C), defined as the effective temperature which produces a heat flux through the wall as

$$T_{sa} = T_e + \frac{1}{h_{se}}[\alpha G_v - \epsilon B_{lw}] \tag{3}$$

where α, ϵ are the wall absorptance and emittance, respectively, and h_{se} (W/m^2 K) is the external surface heat transfer coefficient.

Then an equation similar to Eq. (1) can be written to include the effect of global vertical solar irradiance and long wave radiation balance as

$$Q = U(T_i - T_{sa}) \tag{4}$$

It must be noted that the operative temperature should be used in Eq. (4) instead of the indoor air ambient temperature [16], but under test conditions in the present work they can be supposed approximately equals.

Thus, the balance equation, taking into account Eqs. (3) and (4), appears with absorptance term separated from other parameters:

$$Q = U\left[T_i - T_e - \frac{\alpha}{h_{se}}G_v + \frac{\epsilon}{h_{se}}B_{lw}\right] \quad (5)$$

$$Q = U(T_i - T_e) - \frac{U\alpha}{h_{se}}G_v + \frac{U\epsilon}{h_{se}}B_{lw} \quad (6)$$

The following relevant relation is observed when comparing Eqs. (2) and (6) [17]:

$$g = \frac{U\alpha}{h_{se}} \quad (7)$$

where the solar energy transmittance is expressed as function of other thermal parameters which is useful to identify them. A similar relation is found to long wave energy transmittance, b, but ϵ is used instead of α.

Finally, it must be noted that steady state analysis applicability is limited [18]. Thus, to obtain equations with general validity in tests carried out under dynamic test conditions, accumulation effects must be added to energy balance equations presented. These dynamic features are considered in next sections.

5.2. Surface heat transfer coefficient

Two important parameters to take into account are the external and internal surface heat transfer coefficient, h_{se} and h_{si}, respectively, which consist in convective as well as radiative components. They are part of the U value by definition [13,16]:

$$\frac{1}{U} = \frac{1}{h_{se}} + \frac{1}{U_d} + \frac{1}{h_{si}} \quad (8)$$

where U_d is the wall design thermal transmittance surface to surface, it is supposed approximately constant.

Most authors consider as h_{se} as h_{si} constants within a range [15]. Here the internal surface heat transfer coefficient, h_{si}, will be supposed approximately constant, and external surface heat transfer coefficient, h_{se}, is modelled as being constant or as a linear dependence of the wind speed, w (m/s):

$$h_{se} = h_{se}(w) \approx k_1 + k_2 w \quad (9)$$

where k_1 and k_2 are supposed constants.

Furthermore, it is studied whether a non-linear relation (w^k) could improve the results.

Eq. (9), in the present work, considers the external surface radiative heat transfer coefficient, h_{re}, as constant and the external surface convective heat transfer coefficient, h_{ce}, as linear dependent on wind speed [16].

This is due to h_{re} can vary between 4 and 6 (W/m^2 K) while the external convective heat transfer coefficient, h_{ce}, can vary largely [4–24] (W/m^2 K) [16,19,20]. Thus, h_{re} variation is supposed negligible in this study.

5.3. External surface temperature

Firstly, it is important to note that the wall is supposed homogeneous and from the experimental conditions is derived that all the significant heat flux throughout the wall is one-dimensional perpendicular to its surface. Secondly, since the involved driving forces of the heat flux passing through the wall follow a pattern dominated by the daily cycle and physical characteristics of the wall are known, the longwave (≈ 1 m) associated to the thermal waves go through the wall is much more than the wall length ($\approx 10^{-1}$ m), and it is permissible the thermo-electrical analogy considering the wall as a single or multiple isothermal nodes using lumped or equivalent thermal parameters [11].

Once introduced hypotheses under is actually assumed the study of the heat flux throughout the wall, an important physical variable to consider is the wall external surface temperature (T_{se} (°C)), from the Fourier's law and the principle of energy conservation, the next equivalent energy balance differential equations can be introduced [21]:

$$C\frac{dT_{wi}}{dt} = U_c A(T_{se} - T_{wi}) + AQ_1 \quad (10)$$

$$C\frac{dT_{wi}}{dt} = U_1 A(T_e - T_{wi}) + \frac{U_1\alpha}{h_{se}}AG_v - \frac{U_1\epsilon}{h_{se}}AB_{lw} + AQ_1 \quad (11)$$

if it is noted that:

$$\frac{1}{U_1} = \frac{1}{h_{se}} + \frac{1}{U_c} \quad (12)$$

$$U_1 = \frac{U_c h_{se}}{U_c + h_{se}} \quad (13)$$

Eq. (11) becomes:

$$\frac{dT_{wi}}{dt} = \frac{U_c h_{se}}{U_c + h_{se}}A(T_e - T_{wi}) + \frac{U_c\alpha}{U_c + h_{se}}AG_v - \frac{U_c\epsilon}{U_c + h_{se}}AB_{lw} + AQ_1 \quad (14)$$

In Eqs. (10)–(14), C (J/K) is effective heat capacity of external part of the wall, T_{se}(°C), T_e(°C) are external surface wall and outdoor air ambient temperatures, respectively, T_{wi}(°C) is the inside temperature of external part of the wall, h_{se} (W/m^2 K) is the external surface heat transfer coefficient, α, ϵ are wall absorptance and emittance, A (m^2) is wall surface, G_v (W/m^2) is the global vertical solar irradiance, B_{lw} (W/m^2) is long wave radiation balance, U_c (W/m^2 K) is the thermal conductance coefficient of external part of the wall and Q_1 (W/m^2) is heat flux density from internal part of the wall.

Combining both Eqs. (11) and (14) is able to obtain the next balance equation:

$$h_{se}(T_e - T_{se}) + U_c(T_{wi} - T_{se}) + \alpha G_v - \epsilon B_{lw} = 0 \quad (15)$$

From Eq. (15) the next relation for the external surface temperature can be derived:

$$T_{se} = \frac{h_{se}}{h_{se} + U_c}T_e + \frac{U_c}{h_{se} + U_c}T_{wi} + \frac{\alpha}{h_{se} + U_c}G_v - \frac{\epsilon}{h_{se} + U_c}B_{lw} \quad (16)$$

Eq. (16) presents useful information about which physical variables wall surface temperature can depend on. This is considered in the following sections.

5.4. Long wave radiation balance

It must be noted that long wave radiation balance, B_{lw} (W/m^2), takes into account that the external surface radiative heat transfer coefficient, h_{re}, is part of the external surface heat transfer coefficient, h_{se}. Thus, B_{lw} multiplied by wall emittance, ϵ, must be understood as an extra heat flow due to thermal radiation to the surroundings from building element [14,22,23]. B_{lw} can be expressed as

$$B_{lw} = F_{ws}\frac{h_{re,ws}}{\epsilon}(T_e - T_{sky}) + F_{wg}\frac{h_{re,wg}}{\epsilon}(T_e - T_{ground}) \quad (17)$$

where F_{ws} and F_{wg} are the view factors wall-sky and wall-ground, ϵ is wall emittance, $h_{re,ws}$ (W/m^2 K) and $h_{re,wg}$ (W/m^2 K) are the external surface radiative heat transfer coefficients wall-sky and wall-ground, and T_e (°C), T_{sky} (°C), T_{ground} (°C) are the outdoor air ambient, sky and ground temperatures, respectively.

In Eq. (15) the external surface heat transfer coefficient, h_{se}, can be written as a sum of their components [22,24], i.e., external surface convective heat transfer coefficient, h_{ce}, and external surface

radiative heat transfer coefficient, h_{re}. Thus, Eq. (15) becomes:

$$h_{ce}(T_e - T_{se}) + U_c(T_{wi} - T_{se}) + \alpha G_v - \epsilon(h_{reo}(T_{se} - T_e) + B_{lw}) = 0 \tag{18}$$

where it is used $h_{reo} = h_{re}/\epsilon$ and $h_{re} = F_{ws}h_{re,ws} + F_{wg}h_{re,wg}$.

The next relation can be derived from Eq. (18):

$$\epsilon(h_{reo}(T_{se} - T_e) + B_{lw}) = \epsilon(\sigma {T_{se}}^4 - G_{lw}) \tag{19}$$

where G_{lw} (W/m^2) is the long wave irradiance and it is used Stefan–Boltzmann's law for long wave radiation from surface wall to surroundings.

When surface wall temperature is greater than outdoor air ambient temperature, $T_{se} > T_e$, can be observed in Eq. (19) that thermal radiation to the surroundings from building element is lower than long wave radiation balance between wall surface and its surroundings $\epsilon B_{lw} < \epsilon(\sigma {T_{se}}^4 - G_{lw})$.

5.5. Grey-box models

Grey-box models based on SDEs are fitted to data in several settings to identify a detailed model of the heat flux and to enable estimation of the physical parameters based on data. The models are stochastic state-space models consisting of a set of system equations (the SDEs) and a set of measurement equations. The models are lumped parameter models. In the following the simplest feasible grey-box model of the heat flux is formed as an illustrative example. The state of the system is represented by a set of state variables, which are estimated and predicted over the period spanned by the data.

A single state is included in this simple illustrative model where it is supposed heat flux is only caused by difference between inside and outside temperatures. The state T_t at time t is representing the temperature of the wall in an SDE describing the dynamics:

$$dT_t = \left[\frac{U_2}{C_1}(T_{e,t} - T_t) + \frac{U_1}{C_1}(T_{i,t} - T_t)\right] dt + \sigma_1 d\omega_t \tag{20}$$

where $T_{e,t}$ and $T_{i,t}$ are measured inputs, and C_1, U_1, U_2 are the physical parameters of the wall. The ω_t is a Wiener process, which is characterised by having normal distributed increments:

$$\omega_{t_k} - \omega_{t_{k-1}} \sim N(0, t_k - t_{k-1}) \tag{21}$$

The $\sigma(\boldsymbol{\theta})$ is a scaling of the incremental variance. The measurement equation in the simple model is

$$Q_{i,t_k} = U_1(T_{i,t_k} - T_{t_k}) + e_{1,t_k} \tag{22}$$

where Q_{i,t_k} is the measured heat flux at time t_k, T_{t_k} is the state, and $e_{1,t_k} \sim N(0, \sigma_e^2)$ is the measurement noise, which is assumed to be normal distributed, hence it is assumed to be a white noise process.

A general form of the stochastic state-space (or grey-box) models used in the present study are formed by the SDE:

$$d\boldsymbol{x}_t = \boldsymbol{f}(\boldsymbol{x}_t, \boldsymbol{u}_t, \boldsymbol{\theta})dt + \boldsymbol{\sigma}(\boldsymbol{\theta})d\boldsymbol{\omega}_t \tag{23}$$

and the measurement equation

$$\boldsymbol{y}_{t_k} = \boldsymbol{h}(\boldsymbol{x}_{t_k}, \boldsymbol{u}_{t_k}, \boldsymbol{\theta}) + \boldsymbol{e}_{t_k} \tag{24}$$

where $\boldsymbol{x}_t$ is the state vector, $\boldsymbol{u}_t$ is the input vector, the parameters are $\boldsymbol{\theta} \in \Theta \subset \Re^p$ and $\boldsymbol{y}_{t_k}$ is the output vector. Hence this is obtained for the simple model above by setting: $\boldsymbol{x}_t = T_t$, $\boldsymbol{u}_t = (T_{i,t}, T_{e,t})$, $\boldsymbol{y}_{t_k} = Q_{i,t_k}$ and $\boldsymbol{\theta} = (C_1, U_1, U_2, \sigma_1, \sigma_e)$.

By using grey-box models the complexity of the model can be increased from the simple model presented above allowing the energy transfer processes occurring to be modeled in more detail based on physical knowledge. Furthermore, the grey-box model setup enables maximum likelihood parameter estimation, as outlined in the following section, and is thereby a statistically based and feature rich approach to fitting physical models to measurement series from the system.

It must be highlighted that the system states which are measured can be included as well as non measured states. This is a very useful feature for modelling physical systems, as the underlying (hidden) processes can be represented with a physical model, while using states which are practically possible to measure. This is very important for identifying physical parameters and proves very useful in the work reported in this paper.

5.6. Maximum likelihood parameter estimation

The SDE based on grey-box models are used for maximum likelihood parameter estimation as outlined in this section. Let the observations be represented by

$$\mathcal{Y}_{t_N} = [\boldsymbol{y}_{t_N}, \boldsymbol{y}_{t_{N-1}}, \ldots, \boldsymbol{y}_{t_1}, \boldsymbol{y}_{t_0}] \tag{25}$$

where $\boldsymbol{y}_{t_k}$ is a vector of the measured model outputs at time t_k. For example, for the simple model outlined in previous section all the measurements of the heat flux up to time t_k is

$$\mathcal{Y}_{t_k} = [Q_{i,t_k}, Q_{i,t_{k-1}}, \ldots, Q_{i,t_1}, Q_{i,t_0}] \tag{26}$$

The likelihood function is the joint probability density

$$L(\boldsymbol{\theta}; \mathcal{Y}_{t_N}) = \left(\prod_{k=1}^{N} p(\boldsymbol{y}_{t_k} | \mathcal{Y}_{t_{k-1}}, \boldsymbol{\theta})\right) p(\boldsymbol{Y}_{t_0} | \boldsymbol{\theta}) \tag{27}$$

where $p(\boldsymbol{y}_{t_k} | \mathcal{Y}_{t_{k-1}}, \boldsymbol{\theta})$ is a conditional density denoting the probability of observing $\boldsymbol{y}_{t_k}$ given the previous observations $\mathcal{Y}_{t_{k-1}}$ and the parameters $\boldsymbol{\theta}$, and where $p(\boldsymbol{Y}_{t_0} | \boldsymbol{\theta})$ is a parameterization of the starting conditions. The maximum likelihood estimates of the parameters are then found by

$$\hat{\boldsymbol{\theta}} = \underset{\boldsymbol{\theta}}{\arg\max}\{L(\boldsymbol{\theta}; \mathcal{Y}_{t_N})\} \tag{28}$$

Due to the previously mentioned assumptions about the noise process, it follows that the conditional densities in Eq. (28) are Gaussian densities.

The likelihood in Eq. (27) can be calculated with a Kalman filter if the model is linear and with an extended Kalman filter if the model is non-linear, and an optimization algorithm can be applied to maximize it, thereby calculating the maximum likelihood estimates, see [25] for a detailed discussion. This is implemented in the computer software CTSM, which has been used for carrying out the parameter estimation, see more about the software at[3] and in [26].

5.7. Confidence intervals for parameters

The applied maximum likelihood estimation of the parameters enables estimation of the parameter uncertainty. The parameter estimator are asymptotically Gaussian with mean $\boldsymbol{\theta}$ and covariance:

$$\boldsymbol{\Sigma}_\theta = \boldsymbol{H}^{-1} \tag{29}$$

where $\boldsymbol{H}$ is the Hessian evaluated at the minimum of the likelihood function, see more in [27] for details on how this is computed in CTSM. The vector $\boldsymbol{\sigma}_\theta$ which is the diagonal of the covariance matrix holds the standard deviations of the parameter estimates. This is used to calculate approximate 95% confidence intervals for the parameters:

$$[\boldsymbol{\theta}_{2.5\%}, \boldsymbol{\theta}_{97.5\%}] = [\hat{\boldsymbol{\theta}} - 2\boldsymbol{\sigma}_\theta, \hat{\boldsymbol{\theta}} + 2\boldsymbol{\sigma}_\theta] \tag{30}$$

[3] http://www.imm.dtu.dk/ ctsm.

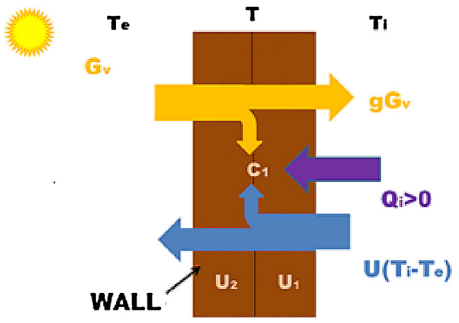

Fig. 6. Balance energy scheme for one-state model.

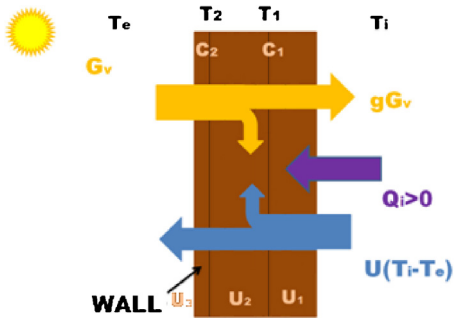

Fig. 7. Balance energy scheme for two-state model.

This is used for all the parameters estimated directly. The confidence interval the U value, which is a non-linear function of a subset of the parameters, is calculated as described in Section 5.9.

5.8. Models

Having studied the mathematical and physical issues, the next step is to present the stochastic differential equation used for parameter estimation with the software CTSM [26,28].

Three possible models are considered, a single state model and a pair of two-state models, which only differ in one measurement equation.

In models are considered:

- Measured variables
  - T_{se}, T_e, T_i(°C) are the exterior surface, outside and inside air temperatures, respectively.
  - Q_i, G_v, B_{lw} (W/m^2) are heat flux density through inside part of the wall, global vertical solar irradiance and long wave radiation balance between wall and its surroundings, respectively.

- State variables
  - T, T_1, T_2(°C) are state temperatures inside the wall.

- Estimated parameters
  - U_1, U_2, U_3, h_{se} (W/m^2 K)) are heat transfer coefficients of part of the wall and external surface heat transfer coefficient, respectively.
  - C_1, C_2($Wmin/m^2K$)) are the effective heat capacities of part of the wall.
  - α, ϵ are wall absorptance and emittance.

5.8.1. Model 1

Fig. 6 shows the energy contributions to the heat flux through the wall.

The state equation considering the energy balance can be written as

$$dT = \left[\frac{U_2}{C_1}(T_e - T) + \frac{U_1}{C_1}(T_i - T) + \frac{U_2\alpha}{C_1 h_{se}}G_v - \frac{U_2\epsilon}{C_1 h_{se}}B_{lw}\right]dt + \sigma_1 d\omega_t \quad (31)$$

where T is a hidden state, which means that it is not measured. In this case the measurement equation is

$$Q_{i,t_k} = U_1(T_{i,t_k} - T_{t_k}) + e_{1,t_k} \quad (32)$$

Two forms of Model 1 is applied:

- m1: assuming a constant h_{se}.
- m1w: assuming h_{se} linear as dependent on wind speed.

5.8.2. Model 2a

Model 2a is created by adding a new state variable to represent the wall surface temperature. Fig. 7 represents the energy balance through the wall with two-state model.

Thus obtaining two equations, one equation for each state:

$$dT_1 = \left[\frac{U_2}{C_1}(T_2 - T_1) + \frac{U_1}{C_1}(T_i - T_1)\right]dt + \sigma_{11}d\omega_t \quad (33)$$

$$dT_2 = \left[\frac{U_3}{C_2}(T_e - T_2) + \frac{U_2}{C_2}(T_1 - T_2) + \frac{U_3\alpha}{C_2 h_{se}}G_v - \frac{U_3\epsilon}{C_2 h_{se}}B_{lw}\right]dt + \sigma_{22}d\omega_t \quad (34)$$

where T_1 is a hidden state.

With the two following measurement equations:

$$Q_{i,t_k} = U_1(T_{i,t_k} - T_{t_k}) + e_{11,t_k} \quad (35)$$

$$T_{se,t_k} = T_{2,t_k} + e_{22,t_k} \quad (36)$$

Model 2a, named as m2a, is studied only considering h_{se} as constant.

5.8.3. Model 2b

This model is defined as Model 2a, but using the following measurement equation instead of Eq. (36):

$$T_{se,t_k} = a_1 T_{e,t_k} + a_2 T_{2,t_k} + a_3 G_{v,t_k} + a_4 B_{lw} + e_{22,t_k} \quad (37)$$

where it is supposed that the wall surface temperature is function of T_e, T_2, G_v and B_{lw} (Section 5.3).

Two forms of Model 2b are considered:

- m2b: assuming a constant h_{se}.
- m2bw: assuming h_{se} linear as dependent on wind speed.

5.9. Obtaining physical parameters

Thus, with these models it is possible to obtain estimates of parameters which describe and characterise the thermal behaviour of the wall.

For models presented α can be identified directly, see Eqs. (31) and (34).

The effective heat capacity of the wall is obtained by

$$C = \sum_i C_i A \quad (38)$$

where C_i (W min/m^2 K) are the effective heat capacities which are estimated and A (m^2) is the known surface of the wall.

The U value is obtained by

$$U(\boldsymbol{\theta}_U) = \frac{1}{\sum_i \frac{1}{\theta_{U,i}}} = \frac{1}{\sum_i \frac{1}{U_i}} \quad (39)$$

where $\boldsymbol{\theta}_U = (U_1, U_2, \ldots, U_n)^T$ is a vector of all the n included U values in the model. As the U value is a non-linear function of a subset of

the parameters the confidence interval for the U value cannot be directly calculated, but has to be approximated. A linear approximation is used as described in the following. In Section 5.7 it is outlined how the covariance matrix for the parameters can be estimated. By taking the variance and covariance of the parameters used in Eq. (39) the covariance matrix for the U value parameters can be formed as

$$\boldsymbol{\Sigma}_{\boldsymbol{\theta_U}} = \begin{pmatrix} \sigma^2_{U_1} & \sigma^2_{U_1,U_2} & \cdots & \sigma^2_{U_1,U_n} \\ \sigma^2_{U_2,U_1} & \sigma^2_{U_2} & \cdots & \sigma^2_{U_2,U_n} \\ \vdots & \vdots & \ddots & \\ \sigma^2_{U_n,U_1} & \sigma^2_{U_n,U_2} & & \sigma^2_{U_n} \end{pmatrix} \tag{40}$$

The uncertainty of the U value is computed by approximating the function of the parameters with a first-order Taylor expansion in matrix form:

$$U(\boldsymbol{\theta}_U) \approx U(\hat{\boldsymbol{\theta}}_U) + J\,\boldsymbol{\theta}_U \tag{41}$$

where J is the Jacobian of the U value function:

$$J = \left(\frac{\partial U(\boldsymbol{\theta}_U)}{\partial U_1}, \frac{\partial U(\boldsymbol{\theta}_U)}{\partial U_2}, \ldots, \frac{\partial U(\boldsymbol{\theta}_U)}{\partial U_n} \right) \tag{42}$$

where

$$\frac{\partial U(\boldsymbol{\theta}_U)}{\partial U_j} = \frac{1}{\left(\sum_{i=1}^{n} \frac{1}{U_i}\right)^2 U_j^2} \tag{43}$$

The variance of the U value is then approximated by

$$\sigma^2_U \approx J\,\boldsymbol{\Sigma}_{\boldsymbol{\theta}_U} J^T \tag{44}$$

which is used to calculate 95% confidence intervals by

$$[U_{2.5\%},\ U_{97.5\%}] = \left[U(\hat{\boldsymbol{\theta}}) - 2\sigma_{U(\boldsymbol{\theta_U})},\ U(\hat{\boldsymbol{\theta}}) + 2\sigma_U \right] \tag{45}$$

6. Results and discussions

In this section the modelling results are presented and discussed. In the first part the considerations on dividing the entire period into twenty-one periods and how a suitable sample period is selected. The balance is between using a too high sample-rate, which results in including not wanted fast dynamic effects, and using a too low sample-rate, which results in removing the dynamic effects describing the needed thermal characteristics of the wall. Following this, it is a part about the inclusion of long wave radiation, and then the presentation of the results from fitting the one-state Model 1 and the two-state Models 2a and 2b. Finally, the results are discussed including the uncertainty estimates.

6.1. Selection of data sets and sample-rate

Data are split in twenty-one data sets with ten days each one along the available period of measurement. The considered data sets used in estimates are summarized in Table 1.

The availability of so many data sets allows to study the feasibility of this analysis for data recorded under the different test conditions, some of them appropriate and other not so good as discussed in Section 4, and also gives an strong support for model validation.

Preliminary, a study with 1 min sample-rate was carried out using Model 1 and data set from series 5 (Table 1), which are recorded with that sample-rate. An analysis of the residuals obtained using this frequency data are shown in Fig. 8. A significant autocorrelation and the cumulated periodogram in the residuals are found for high frequencies. It reveals that some periodicity in the signal is present with a frequency around $(1/8)\,\text{min}^{-1}$, which is most likely due to the thermostatic control of the indoor temperature.

Thus, the residuals analysis shows that the 1 min sample-rate is not a suitable choice, because describing the oscillations in these ranges are not relevant for the objectives of identifying the thermal behaviour of the wall.

Hence, several lower sample-rates were checked to identify the most appropriate to evaluate this wall in particular. The best results were obtained taking a 30 min sample-rate. It was also considered a good sample-rate to study physical phenomena that affects a building component because of the dynamic thermal behaviour of the wall is not lost. Then, although the wall is better controlled and monitored with higher sample-rates, to have a better description itself the posterior analysis is done with lower sample-rates without losing accuracy.

6.2. Long wave radiation balance term

In Section 5.4 was showed that term related to long wave radiation balance, B_{lw} (W/m^2), between building element and its surroundings is usually seen as an extra heat flow due to thermal radiation to the surroundings from building element, and it depends on difference between the external air temperature and the apparent surroundings temperature.

In the present work, test experiment conditions imply that wall surface temperature is greater than outdoor air ambient temperature, $T_{se} > T_e$, most times except in some summer night periods, Fig. 5. Thus, $(\sigma {T_{se}}^4 - G_{lw}) > B_{lw}$ was taken as approach to check if long wave term could be considered negligible for the vertical wall studied [15].

On this way, using this maximum value $(\sigma {T_{se}}^4 - G_{lw})$ instead of B_{lw}, long wave radiation effect was observed negligible in preliminary results and likelihood ratio tests [10]. Hence in all presented results this effect is not included in the models to the present work.

Nonetheless, long wave radiation effect should be taken into account in future studies when experiment conditions are different. Besides, it would be interesting to study this effect in summer night periods in detail.

In these cases, if long wave irradiance, G_{lw}, measurements are available, Eq. (46) could be used instead of Eq. (17):

$$B_{lw} = F_{wsg} \frac{h_{re,wsg}}{\epsilon} (T_e - T_{sg}) \tag{46}$$

where F_{wsg} is the view factor wall-surroundings, ϵ is wall emittance, $h_{re,wsg}$ (W/m^2 K) is the external surface radiative heat transfer coefficient wall-surroundings and T_{sg} is the surroundings temperature, which can be derived from expression: $G_{lw} = \sigma {T_{sg}}^4$, where pyranometer emittance is supposed unity.

6.3. Model 1

First, Model 1 was used to make a complete study of the wall in order to obtain the parameters, which characterise it, using all each of the data sets listed in Table 1.

6.3.1. Parameter estimates

Parameters calculated are shown in Table 2 when h_{se} is supposed constant and in Table 3 when it is supposed linear dependent on wind speed (Fig. 13).

Presented values correspond to U value, U (W/m^2 K), Loglikelihood, Loglik, effective heat capacity, C (J/K), and absorptance, α. The estimated uncertainties of the parameters for each time series are specified as $\pm 2\sigma_{\theta_i}$ indicating the 95% confidence intervals.

In order to show how the variation of the parameters is along the present study for Model 1, the mean values of series 1–21 are used,

Table 2
Model 1. Estimated parameters with h_{se} constant.

Series	U (W/m^2 K)	Loglik	C (J/K)	α
01	1.965 ± 0.037	−893	$(1.19 \pm 0.19) \times 10^6$	0.76 ± 12.12
02	1.984 ± 0.023	−829	$(5.95 \pm 0.48) \times 10^5$	0.75 ± 06.62
03	2.097 ± 0.033	−919	$(7.73 \pm 0.77) \times 10^5$	0.76 ± 11.68
04	2.065 ± 0.031	−900	$(7.53 \pm 0.75) \times 10^5$	0.76 ± 09.05
05	2.003 ± 0.031	−824	$(7.29 \pm 0.69) \times 10^5$	0.76 ± 09.54
06	2.038 ± 0.046	−728	$(7.82 \pm 0.75) \times 10^5$	0.76 ± 02.44
07	2.046 ± 0.042	−912	$(6.52 \pm 0.61) \times 10^5$	0.74 ± 07.79
08	1.966 ± 0.032	−672	$(9.47 \pm 0.68) \times 10^5$	0.68 ± 02.56
09	1.941 ± 0.033	−605	$(9.32 \pm 0.59) \times 10^5$	0.66 ± 02.24
10	1.981 ± 0.042	−655	$(1.18 \pm 0.22) \times 10^6$	0.72 ± 05.76
11	2.104 ± 0.080	−824	$(6.48 \pm 0.54) \times 10^5$	0.60 ± 00.01
12	2.077 ± 0.079	−829	$(6.22 \pm 0.43) \times 10^5$	0.73 ± 02.87
13	1.953 ± 0.105	−758	$(6.55 \pm 0.38) \times 10^5$	0.75 ± 06.70
14	2.247 ± 0.127	−736	$(6.28 \pm 0.36) \times 10^5$	0.76 ± 04.33
15	2.253 ± 0.120	−855	$(6.26 \pm 0.40) \times 10^5$	0.76 ± 05.84
16	2.589 ± 0.100	−1003	$(6.61 \pm 0.52) \times 10^5$	0.76 ± 10.15
17	1.996 ± 0.189	−1003	$(6.39 \pm 0.40) \times 10^5$	0.76 ± 21.43
18	2.145 ± 0.388	−979	$(6.19 \pm 0.40) \times 10^5$	0.77 ± 03.90
19	1.547 ± 0.347	−961	$(5.18 \pm 0.11) \times 10^5$	0.77 ± 01.88
20	1.877 ± 0.334	−987	$(5.67 \pm 0.61) \times 10^5$	0.76 ± 10.21
21	2.143 ± 0.328	−948	$(6.76 \pm 0.74) \times 10^5$	0.75 ± 10.11
Average	2.048 ± 0.372		$(7.33 \pm 3.59) \times 10^5$	0.74 ± 00.08

Table 3
Model 1. Estimated parameters with h_{se} dependent on wind speed.

Series	U (W/m^2 K)	Loglik	C (J/K)	α
01	1.961 ± 0.037	−820	$(8.90 \pm 6.97) \times 10^5$	0.77 ± 07.50
02	1.997 ± 0.024	−808	$(6.23 \pm 0.47) \times 10^5$	0.68 ± 00.03
03	2.105 ± 0.029	−853	$(7.89 \pm 0.73) \times 10^5$	0.77 ± 00.06
04	2.065 ± 0.031	−885	$(7.44 \pm 0.78) \times 10^5$	0.78 ± 00.09
05	2.012 ± 0.034	−814	$(7.66 \pm 0.76) \times 10^5$	0.76 ± 00.24
06	2.046 ± 0.047	−720	$(7.83 \pm 0.75) \times 10^5$	0.72 ± 00.04
07	2.060 ± 0.045	−904	$(6.66 \pm 0.66) \times 10^5$	0.77 ± 00.13
08	1.967 ± 0.039	−671	$(9.50 \pm 0.67) \times 10^5$	0.77 ± 00.09
09	1.943 ± 0.034	−604	$(9.37 \pm 0.62) \times 10^5$	0.77 ± 00.74
10	1.994 ± 0.044	−639	$(1.22 \pm 0.31) \times 10^6$	0.77 ± 00.06
11	1.580 ± 0.064	−819	$(6.56 \pm 0.55) \times 10^5$	0.77 ± 01.38
12	1.631 ± 0.033	−829	$(6.22 \pm 0.44) \times 10^5$	0.77 ± 01.14
13	1.686 ± 0.029	−758	$(6.55 \pm 0.40) \times 10^5$	0.77 ± 00.03
14	1.714 ± 0.035	−736	$(6.28 \pm 0.37) \times 10^5$	0.80 ± 01.94
15	1.751 ± 0.041	−855	$(6.28 \pm 0.40) \times 10^5$	0.77 ± 00.03
16	1.774 ± 0.054	−1011	$(6.50 \pm 0.58) \times 10^5$	0.79 ± 04.11
17	1.795 ± 0.045	−1002	$(6.45 \pm 0.41) \times 10^5$	0.79 ± 00.03
18	1.863 ± 0.056	−978	$(6.22 \pm 0.40) \times 10^5$	0.80 ± 00.06
19	1.903 ± 0.137	−959	$(5.04 \pm 1.14) \times 10^5$	0.80 ± 04.24
20	1.781 ± 0.393	−985	$(5.67 \pm 0.65) \times 10^5$	0.71 ± 00.10
21	2.083 ± 0.351	−940	$(6.76 \pm 0.69) \times 10^5$	0.76 ± 00.09
Average	1.895 ± 0.311		$(7.25 \pm 3.17) \times 10^5$	0.77 ± 00.06

as they were equally distributed, to give average value and standard deviation for all parameters, $\overline{X} \pm 2\sigma_X$. U value and absorptance are drawn in Fig. 13.

U value coefficient of variation, $\sigma_U/\overline{U}$, is about 9% when h_{se} is supposed constant, Table 2, and about 8% when h_{se} is considered linear dependent on wind speed, Table 3.

Absorptance presents a coefficient of variation, $\sigma_\alpha/\overline{\alpha}$, about 11% when h_{se} is supposed constant, Table 2, and about 8% when h_{se} is considered linear dependent on wind speed, Table 3.

Lastly, effective heat capacity coefficient of variation, $\sigma_C/\overline{C}$, is about 24% when h_{se} is supposed constant, Table 2, and about 22% when h_{se} is considered linear dependent on wind speed, Table 3.

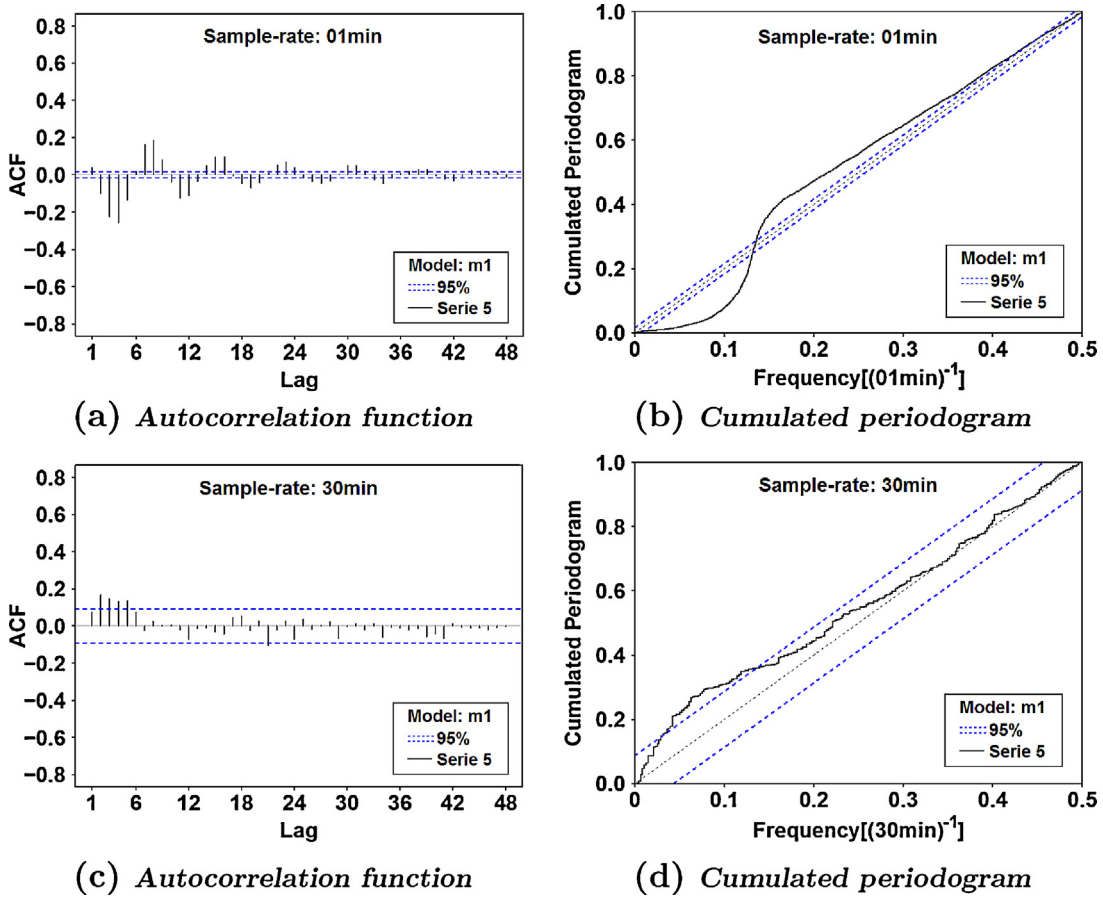

Fig. 8. Analysis Q_i residuals to different sample-rate. Serie 5 (4–13th April).

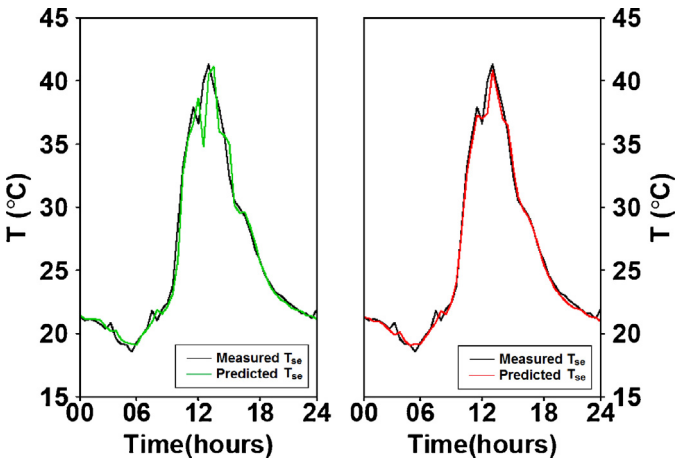

Fig. 9. External surface temperature measured and one-step ahead predicted values using Model 2b: m2b (left) vs. m2a (right). 16th August.

Table 4
Model 2b. Estimated parameters with h_{se} constant.

Series	U (W/m^2 K)	Loglik	C (J/K)	α
01	1.900 ± 0.031	−1464	(1.33 ± 0.23) × 10^6	0.68 ± 05.67
02	1.873 ± 0.051	−1790	(4.59 ± 2.10) × 10^6	0.65 ± 09.61
03	2.226 ± 0.297	−2122	(4.44 ± 3.97) × 10^6	0.69 ± 04.81
04	2.073 ± 0.057	−1490	(1.10 ± 0.16) × 10^6	0.68 ± 03.82
05	1.999 ± 0.035	−1295	(8.66 ± 0.93) × 10^5	0.69 ± 04.68
06	2.046 ± 0.046	−1167	(9.51 ± 1.05) × 10^5	0.68 ± 13.47
07	2.054 ± 0.041	−1376	(8.64 ± 1.03) × 10^5	0.67 ± 12.37
08	2.075 ± 0.057	−1207	(1.11 ± 0.21) × 10^6	0.65 ± 10.43
09	2.024 ± 0.043	−1134	(7.56 ± 0.95) × 10^5	0.63 ± 06.04
10	2.014 ± 0.047	−1065	(9.50 ± 1.40) × 10^5	0.66 ± 07.33
11	1.607 ± 0.137	−1107	(6.24 ± 0.66) × 10^5	0.68 ± 12.04
12	1.561 ± 0.091	−1014	(5.98 ± 0.47) × 10^5	0.69 ± 01.33
13	1.391 ± 0.087	−1013	(5.73 ± 0.48) × 10^5	0.70 ± 13.71
14	1.527 ± 0.123	−946	(5.89 ± 0.59) × 10^5	0.70 ± 10.13
15	1.673 ± 0.132	−1219	(5.87 ± 0.69) × 10^5	0.69 ± 11.17
16	1.752 ± 0.172	−1403	(7.12 ± 1.87) × 10^5	0.69 ± 04.85
17	1.509 ± 0.137	−1360	(5.63 ± 0.67) × 10^5	0.70 ± 14.29
18	2.004 ± 0.130	−1509	(1.39 ± 0.24) × 10^6	0.68 ± 03.57
19	1.950 ± 0.219	−1462	(1.17 ± 1.08) × 10^6	0.68 ± 02.76
20	2.107 ± 0.139	−1616	(1.29 ± 0.13) × 10^6	0.67 ± 02.10
21	2.180 ± 0.146	−1673	(1.43 ± 0.27) × 10^6	0.66 ± 03.47
Average	1.883 ± 0.479		(1.26 ± 2.19) × 10^6	0.68 ± 00.04

Table 5
Model 2b. Estimated parameters with h_{se} dependent on wind speed.

Series	U (W/m^2 K)	Loglik	C (J/K)	α
01	1.914 ± 0.019	−1376	(1.65 ± 0.29) × 10^6	0.55 ± 00.41
02	1.969 ± 0.017	−1608	(1.60 ± 0.37) × 10^6	0.51 ± 00.07
03	2.217 ± 0.208	−2101	(3.85 ± 2.35) × 10^6	0.67 ± 05.00
04	2.073 ± 0.025	−1466	(1.04 ± 0.12) × 10^6	0.59 ± 06.99
05	1.999 ± 0.021	−1244	(8.39 ± 0.78) × 10^5	0.60 ± 00.05
06	2.038 ± 0.043	−1136	(9.13 ± 0.93) × 10^5	0.51 ± 00.10
07	2.073 ± 0.041	−1352	(9.11 ± 1.00) × 10^5	0.50 ± 00.01
08	2.117 ± 0.063	−1213	(1.42 ± 0.27) × 10^6	0.50 ± 00.01
09	2.069 ± 0.074	−1163	(9.65 ± 3.09) × 10^5	0.50 ± 00.01
10	2.026 ± 0.048	−1034	(9.77 ± 1.30) × 10^5	0.50 ± 00.01
11	1.594 ± 0.103	−1142	(7.06 ± 0.70) × 10^5	0.50 ± 00.01
12	1.672 ± 0.052	−1054	(6.90 ± 0.67) × 10^5	0.50 ± 00.01
13	1.718 ± 0.033	−1069	(7.13 ± 0.66) × 10^5	0.50 ± 00.01
14	1.713 ± 0.028	−973	(6.66 ± 0.57) × 10^5	0.50 ± 00.01
15	1.779 ± 0.035	−1229	(6.62 ± 0.60) × 10^5	0.50 ± 00.01
16	1.735 ± 0.189	−1415	(7.30 ± 2.35) × 10^5	0.52 ± 00.11
17	1.737 ± 0.058	−1350	(6.85 ± 0.58) × 10^5	0.54 ± 00.06
18	1.852 ± 0.095	−1501	(8.81 ± 2.92) × 10^5	0.50 ± 00.04
19	1.816 ± 0.053	−1467	(8.67 ± 3.07) × 10^5	0.50 ± 00.01
20	1.920 ± 0.067	−1640	(2.80 ± 0.33) × 10^6	0.58 ± 00.08
21	1.938 ± 0.094	−1635	(8.70 ± 2.91) × 10^5	0.50 ± 00.01
Average	1.903 ± 0.332		(1.16 ± 1.54) × 10^6	0.53 ± 00.09

Table 6
Likelihood ratio test. Notation: submodel⊂model, Model 1: h_{se} constant (m1) and dependent on wind speed (m1w). Model 2b: h_{se} constant (m2b) and dependent on wind speed (m2bw) for Q_i and T_{se} outputs.

Series	m1 ∩ m1w	m1 ∩ m2b	m1w ∩ m2b	m1 ∩ m2bw	m1w ∩ m2bw	m2b Q_i ∩ m2bw Q_i	m2b T_{se} ∩ m2bw T_{se}
01	0.00	0.00	0.00	0.00	0.00	0.00	0.00
02	0.00	1.00	1.00	0.00	0.00	0.00	1.00
03	0.00	1.00	1.00	1.00	1.00	0.00	0.00
04	0.00	0.00	0.00	0.00	0.00	0.04	0.00
05	0.00	0.00	0.00	0.00	0.00	1.00	0.00
06	0.00	0.00	0.00	0.00	0.00	1.00	0.00
07	0.00	0.00	0.00	0.00	0.00	1.00	0.00
08	0.48	1.00	1.00	1.00	1.00	1.00	1.00
09	0.40	1.00	1.00	1.00	1.00	1.00	1.00
10	0.00	0.00	0.00	0.00	0.00	0.00	0.00
11	0.00	0.00	0.00	0.00	0.00	1.00	1.00
12	1.00	0.00	0.00	0.00	0.00	1.00	0.00
13	1.00	0.00	0.00	0.00	0.00	1.00	1.00
14	0.43	0.00	0.00	0.00	0.00	1.00	1.00
15	0.49	0.00	0.00	0.00	0.00	1.00	1.00
16	1.00	0.00	0.00	0.00	0.00	1.00	0.00
17	0.32	0.00	0.00	0.00	0.00	1.00	0.00
18	0.35	0.00	0.00	0.00	0.00	1.00	0.00
19	0.05	0.00	0.00	0.00	0.00	0.15	1.00
20	0.06	0.00	0.00	0.00	0.00	1.00	1.00
21	0.00	0.00	0.00	0.00	0.00	0.00	0.00

Another results obtained using a non-linear dependence on wind, as $k_1 w^{k_2}$, were tried but for this wall the better fits were obtained when k_2 is equal to one or zero.

6.3.2. Qi one-step ahead prediction validation

Results obtained were validated using the one-step ahead prediction residuals for all series to verify if the condition of white noise residuals is fulfilled. Fig. 10 shows autocorrelation and cumulated periodogram of the residuals, where is able to see that the residuals behaviour improves for most series when h_{se} linear dependent on wind speed is considered.

A good fit has been achieved with all data series along different periods within different seasons, and it is important that parameter values considering their confidence intervals are in similar ranges. Another important aspect is that a good residuals analysis was observed using all data sets recorded under different meteorological conditions, though a problem is observed at frequencies corresponding to multiples of one day period, since lines in cumulated periodogram are above confidence interval for these frequencies.

6.4. Models 2a and 2b

Model 2a is created by adding a new state variable to represent the wall surface temperature. As shown in the following the measurement equation describing the measured wall surface temperature needs to be refined, as carried out in Model 2b.

Model 2a presents a problem when measured and predicted values, obtained using CTSM, are compared. The measurement equation cause the second state, T_2 (°C), to be defined as the measured wall surface temperature, Eq. (36), and this implies that the effective heat capacity is associated to the surface temperature, T_{se} (°C), in the lumped model. In order to lump the model in an alternative way to solve the observed problem, the second state represents a temperature inside the wall and it is necessary to use the measurement equation of Model 2b, Eq. (37), which implies that the effective heat capacity associated to the surface temperature, T_{se} (°C), is negligible [21]. In Model 2b the measured surface temperature depends on state variable, T_2 (°C), the solar global vertical irradiance, G_v (W/m^2), the outside air temperature T_e (°C)

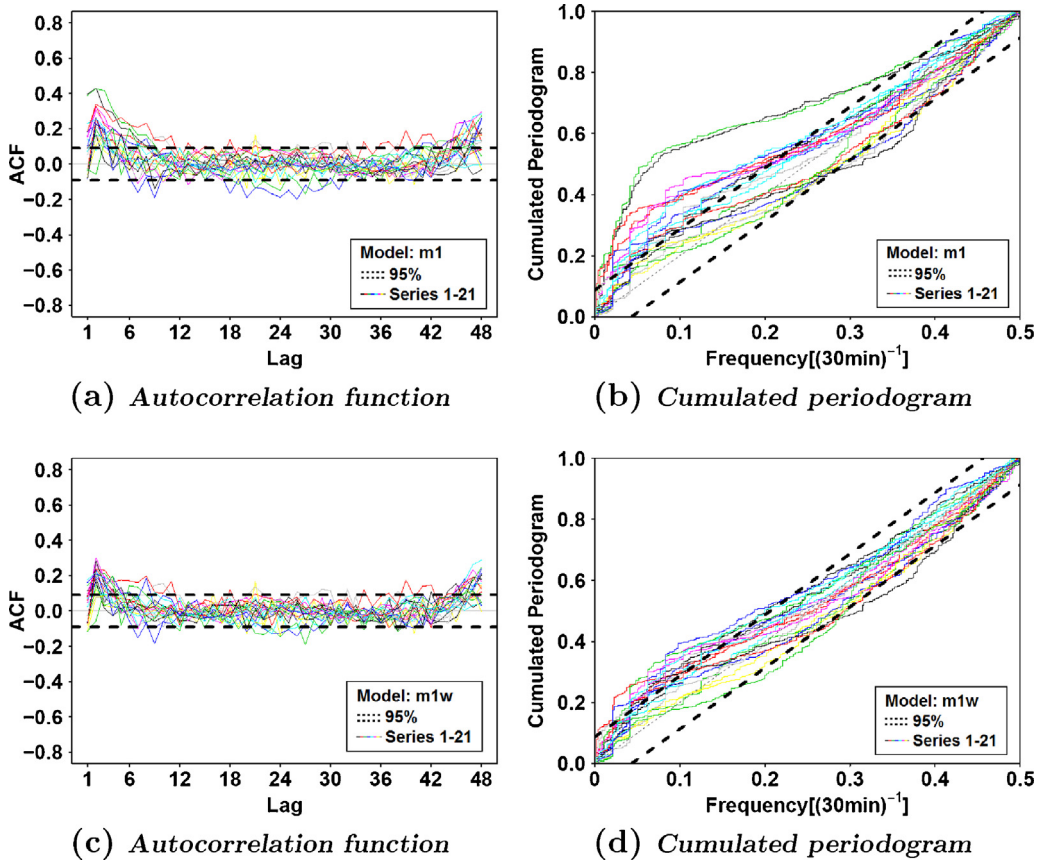

Fig. 10. Analysis Q_i residuals. Model 1 h_{se} constant (m1) and dependent on wind speed (m1w).

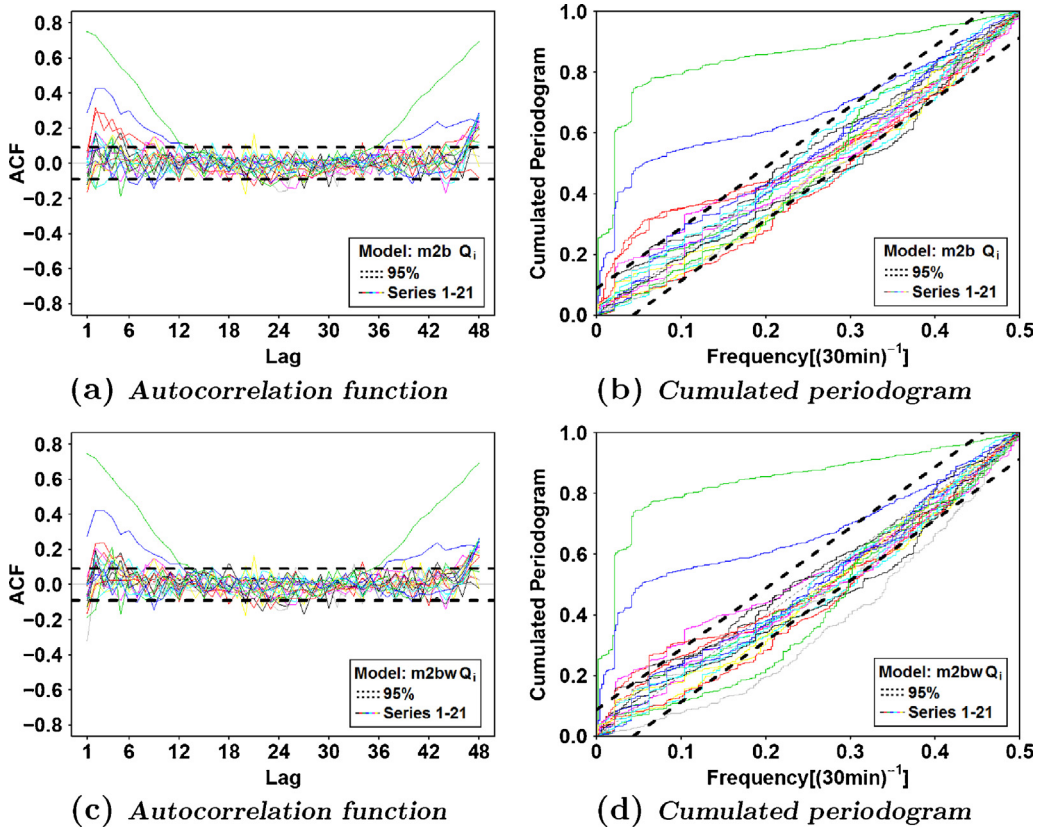

Fig. 11. Analysis Q_i residuals. Model 2b h_{se} constant (m2b) and dependent on wind speed (m2bw). (For interpretation of the references to color in this figure legend, the reader is referred to the web version of the article.)

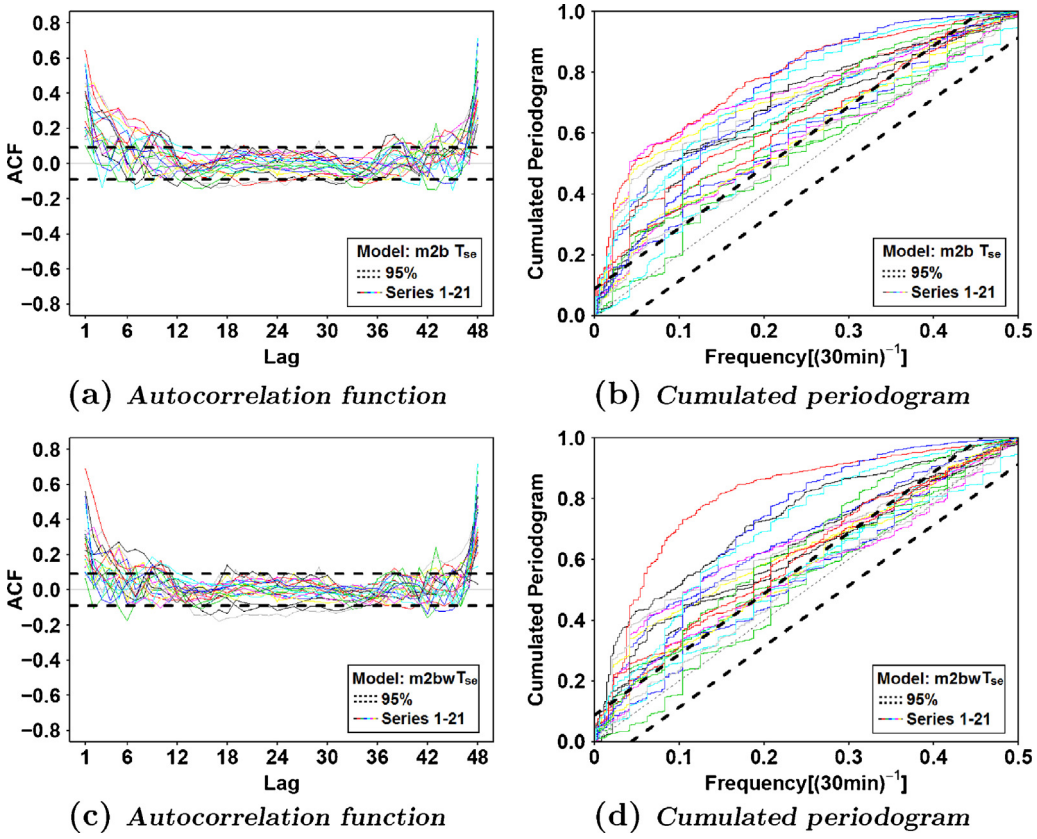

Fig. 12. Analysis T_{se} residuals. Model 2b h_{se} constant (m2b) and dependent on wind speed (m2bw).

and the extra long wave radiation energy balance, B_{lw} (W/m^2). The likelihood for all periods increased significantly using Model 2b over Model 2a. In Fig. 9 the measured and predicted values to the wall surface temperature is shown for a single day to illustrate that the Model 2b is better for describing the wall surface temperature.

6.4.1. Parameter estimates

Model 2b was used to estimate the parameters for all the data sets. As Model 1, parameter values were estimated assuming h_{se} as constant, Table 4, and considering h_{se} as linear dependent on wind speed, Table 5 (Fig. 13).

The presented values also correspond to U value, U (W/m^2 K), Loglikelihood, Loglik, effective heat capacity, C (J/K), and absorptance, α. The estimated uncertainties of the parameters for each time series are specified as $\pm 2\sigma_{\theta_i}$ indicating the 95% confidence intervals.

In order to show how the variation of the parameters is along the present study for Model 2b, the mean values of series 1–21 are used, as they were equally distributed, to give average value and standard deviation for all parameters, $\overline{X} \pm 2\sigma_X$. U value and absorptance are drawn in Fig. 13.

U value coefficient of variation, $\sigma_U/\overline{U}$, is about 13% when h_{se} is supposed constant, Table 4, and about 9% when h_{se} is linear dependent on wind speed, Table 5.

Absorptance presents a coefficient of variation, $\sigma_\alpha/\overline{\alpha}$, about 5% when h_{se} is supposed constant, Table 2, and about 17% when h_{se} is considered linear dependent on wind speed, Table 3.

Lastly, effective heat capacity coefficient of variation, $\sigma_C/\overline{C}$, is higher than 50% in both cases, h_{se} supposed constant, Table 2, and h_{se} considered linear dependent on wind speed, Table 3.

6.4.2. Q_i and T_{se} one-step ahead prediction validation

A wide analysis of the one-step ahead residuals was carried out to evaluate range of validity and if the parameters obtained are significant. Both one-step ahead predictions of outputs Qi and Tse are used.

As for Model 1, results obtained were validated using white noise test to the prediction errors. Residuals analysis for all data sets in different months along the recorded data period are presented.

For this model validation taking into account the autocorrelation and the cumulated periodogram of the residuals was carried out for outputs Q_i and T_{se} using the parameter values obtained for each data set. Residuals analysis with h_{se} constant and linear dependent on wind speed is considered both outputs Q_i and T_{se} and it is shown in Figs. 11 and 12, respectively.

A good fit was found using the two-state model, similarly as for the one-state model for most of data sets. Characteristic parameters into similar range considering their confidence intervals have been estimated. Nonetheless, residuals analysis showed at frequencies corresponding to multiples of one day period a worse behaviour than for Model 1, mainly for output T_{se}.

6.5. Likelihood ratio tests

Finally, loglikelihood ratio tests [10] were carried out to check if the improvement of the more complex models is also significantly better for describing the thermal characteristics of the wall, Table 6, where it is indicated when a model(submodel) is less complex than another model(model): *submodel* $\subset$ *model*.

When the p-value is below 5% ($p < 0.05$) for a period, the improvement in likelihood of using a more complex model is significant. For most periods, the results in Table 6 show that the better models are those which consider dependence on wind speed

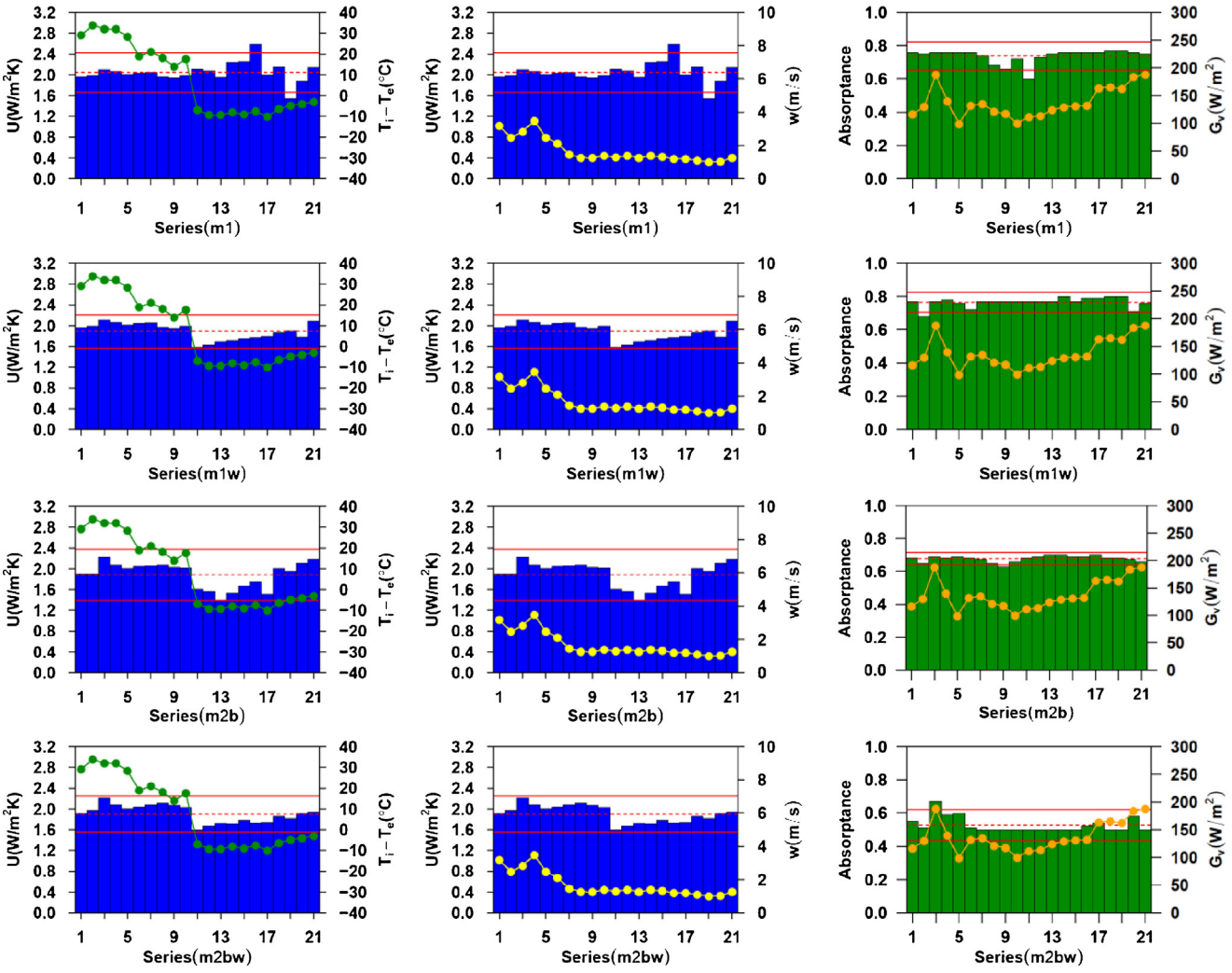

Fig. 13. Estimated parameter values for series 1–21. Red lines show $\overline{X} \pm 2\sigma_X$. Model 1 h_{se} constant (m1) and dependent on wind speed (m1w). Model 2b h_{se} constant (m2b) and dependent on wind speed (m2bw). *U* values are shown besides mean values of gradient temperatures (green) and wind speed (yellow). Absorptance besides mean values of irradiance (orange). (For interpretation of the references to color in this figure legend, the reader is referred to the web version of the article.)

and it is also observed that the two-state models seem to improve regarding the one-state models.

6.6. Discussion

Based on the parameter estimation results it is found that in order to obtain the most important parameters, which describe the thermal behaviour of the wall, a single state model can be considered adequate. Nevertheless, the two-state model can be used in order to achieve a more detailed characterisation of the wall.

It is possible to use models of more than two-state, however a three state model was used for estimation and the obtained results did not improve the likelihood and the white noise properties of the residuals. It is found that the more complex model, which were tried, were overparameterized. In all the studied models for this wall it was observed that terms related to long wave energy exchange with surroundings seemed not significant in most cases.

In Fig. 13 can be observed that the *U* value estimates are close to previous work estimates [1]. Regarding the first period (series 1–10) lower values are seen for some of the series in the second period (series 11–17). This effect could be explained in part for lower values in wind speed (Section 5.2) but it needs to be further investigated. It could be attributed to the poor quality of the signal to noise ratio, that the main measurements present in this second period due to the test and weather conditions, as discussed in Section 4, especially the effect of the shift in temperature gradient, as can be seen in Fig. 13, from the first to the second period. It also could be related with non negligible long wave effect when temperature gradient is low and condition stated in Section 6.2 cannot be supposed.

The level of the estimated effective heat capacity varies widely along all series and it has a high relative dispersion. It can be noted that variation is higher between series for Model 2b. It should be studied more detailed in future works.

Regarding the absorptance, although all models give estimates within the range provided by literature [15], the best performance is observed in Model 2b (m2b) considering the lowest relative dispersion estimates for the different data series as can be seen in Fig. 13, and it must be noted that models without wind dependence in h_{se} present a high correlation between absorptance and external surface heat transfer coefficient. There are also differences in the estimated level of absorptance between the models which varies widely, and it must be studied in next works.

A comparison of the estimated uncertainties for the physical parameters listed for each period for each model in Tables 2–5 supports the conclusions drawn above related to some

fundamental change between the first period and the second period. The uncertainty increases for the last series, which is very reasonable, since the signal to noise ratio decreases as discussed in Section 4.

Finally, the white-noise properties of the residuals obtained for all time series have been studied. The autocorrelation and cumulated periodogram of the residuals for Model 1 show an improvement when h_{se} linear dependent on wind speed is supposed, Fig. 10. This improvement is also found for Model 2b in Figs. 11 and 12, however it is less clear. Problems at frequencies corresponding to multiples of one day period have been observed mainly in Model 2b for output T_{se}. Particularly, the green and blue lines in Fig. 11, which are for series 3 and 4 (Table 1), clearly indicate that the residuals from these series are significantly different from white noise to mentioned frequencies, which is not improved by inclusion of wind speed in h_{se}.

In Fig. 13.

7. Conclusions

Dynamic study of thermal behaviour of simple light wall, which is supposed to be homogeneous, has been applied to obtain the physical parameters that describe the thermal characteristics of the wall using system identification techniques and stochastic differential equations, in order to improve estimations obtained in a previous work using averages method. Results were obtained with the software CTSM.

One-state and two-state models were used to analyse in detail, along nine months with recorded data organized in twenty-one data sets, the wall thermal behaviour estimating: U value, absorptance and effective heat capacity. The different models provide coherent values for physical parameters and a statistical analysis of the one-step ahead residuals was carried out obtaining satisfactory results for different meteorological and test conditions, but they must be improved in future works.

Models considering external surface heat transfer coefficient, h_{se}, linear dependent on wind speed provide the best results and two-state model is able to predict wall surface temperature. Both one and two-state models could be used, since difference between results obtained from them are not significant. All the models considered revealed that long wave energy exchange with surroundings seemed not significant for most time series studied.

U value estimates both one and two-state models are in accordance to those obtained for the same wall applying the linear regression averages method. The main improvement using the presented grey-box modelling approach presented is regarding the period required to estimate the parameters, which is drastically reduced, overcoming the main drawback of that linear regression averages method that frequently require long test periods. Other step forward reported in the present paper, compared to averages method, is giving an estimate of the wall absorptance and wall effective heat capacity.

Model validation was carried out using statistical tests for white noise properties of the one ahead step prediction residuals, and results of the mathematical tests were improved in a wide range of data sets recorded under real weather variable conditions when h_{se} was considered linear dependent on wind speed.

The present paper reports a comprehensive study with good and contrasted results supported by a large amount of data under different weather and test conditions for a system based on a simple light and supposed homogeneous wall.

The method presented states a way to improve averages method which was used to study the same simple an homogeneous wall, and it could provide an useful basis on grey-box modelling to identify parameters which characterise thermal behaviour of building elements. And it also offers to future works the capability to model thermal behaviour using a whole model consistent with international standards.

Particularly, it would be possible to test different walls composed by different materials using grey-box models flexibility under different test conditions. Thus, it could be feasible trying to implement a standard method to characterise in situ building elements.

Acknowledgements

The PSE-ARFRISOL, Reference PS-120000-2005-1, is Strategic Singular Scientific and Technological Project supported by the Spanish Ministry of Science and Innovation and former Ministry of Education and Science approved into the National Plan 2004–2007, co-financed by FEDER funds. The authors wish to thank this support and all the members of the PSE-ARFRISOL consortium for their collaboration.

This work was also supported in part by the Spanish Government under project TEC2012-38883-C02-02 and the French Research Agency (ANR) in the project AIDE-3D.

The Institute of Mathematical Modelling at Technical University of Denmark for human and technical support.

References

[1] I. Naveros, M.J. Jiménez, M.R. Heras, Analysis of capabilities and limitations of the regression method based in averages, applied to the estimation of the U value of building component tested in Mediterranean weather, Energy and Buildings (2012), http://dx.doi.org/10.1016/j.enbuild.2012.09.028.

[2] J.J. Bloem, Workshop on Application of System Identification in Energy Savings in Buildings, October 25–27, 1993, Commission of the European Communities, Joint Research Centre and Institute for Systems Engineering and Informatics (ISPRA), Office Publ. of the Europ. Communities, 1994.

[3] J.J. Bloem, System Identification Competition, EUR (Series), Commission of the European Communities, Joint Research Centre and Institute for Systems Engineering and Informatics (ISPRA), Office Publ. of the Europ. Communities, 1996.

[4] P. Strachan, P. Baker, Outdoor testing, analysis and modelling of building components, Building and Environment 43 (2) (2008) 127–128, special issue in outdoor testing, analysis and modelling of building components, doi:10.1016/j.buildenv.2006.10.008.

[5] H. Madsen, J. Holst, Estimation of continuous-time models for the heat dynamics of a building, Energy and Buildings 22 (1) (1995) 67–79, http://dx.doi.org/10.1016/0378-7788(94)00904-X.

[6] M.J. Jiménez, H. Madsen, Models for describing the thermal characteristics of building components, Building and Environment 43 (2) (2008) 152–162, special issue in outdoor testing, analysis and modelling of building components, doi:10.1016/j.buildenv.2006.10.029.

[7] M.J. Jiménez, B. Porcar, M.R. Heras, Application of different dynamic analysis approaches to the estimation of the building component U value, Building and Environment 44 (2) (2009) 361–367, http://dx.doi.org/10.1016/j.buildenv.2008.03.010.

[8] M.J. Jiménez, H. Madsen, J.J. Bloem, B. Dammann, Estimation of non-linear continuous time models for the heat exchange dynamics of building integrated photovoltaic modules, Energy and Buildings 40 (2) (2008) 157–167, http://dx.doi.org/10.1016/j.enbuild.2007.02.026.

[9] C. Lodi, P. Bacher, J. Cipriano, H. Madsen, Modelling the heat dynamics of a monitored test reference environment for building integrated photovoltaic systems using stochastic differential equations, Energy and Buildings 50 (0) (2012) 273–281, http://dx.doi.org/10.1016/j.enbuild.2012.03.046.

[10] P. Bacher, H. Madsen, Identifying suitable models for the heat dynamics of buildings, Energy and Buildings 43 (7) (2011) 1511–1522, http://dx.doi.org/10.1016/j.enbuild.2011.02.005.

[11] A. Rabl, Parameter estimation in buildings: methods for dynamic analysis of measured energy use, Journal of Solar Energy Engineering 110 (1) (1988) 52–66, http://dx.doi.org/10.1115/1.3268237.

[12] J.D. Guzmán, S. Castaño, M.J. Jiménez, M.R. Heras, Instalación experimental para caracterización del comportamiento térmico de fachadas ventiladas, I Congreso sobre Arquitectura Bioclimática y Frío Solar, Aguadulce, Almeria, Spain, 23–26 March, no. 1, 2010, ISBN: 978-84-693-5141-3.

[13] Thermal Insulation – Building Elements – In-situ Measurement of Thermal Resistance and Thermal Transmittance, International Standard, EN ISO 9869, 1994.

[14] Energy Performance of Buildings. Calculation of Energy Use for Space Heating and Cooling, International Standard, EN ISO 13970, 2007.

[15] P.W. O'Callaghan, S.D. Probert, Sol–air temperature, Applied Energy 3 (4) (1977) 307–311, http://dx.doi.org/10.1016/0306-2619(77)90017-4.
[16] Building Components and Building Elements. Thermal Resistance and Thermal Transmittance. Calculation Method, International standard, EN ISO 6946, 2007.
[17] R. Parsons, R. American Society of Heating, A.-C. Engineers, ASHRAE Handbook: Fundamentals, ASHRAE, 1997.
[18] P. Baker, H. van Dijk, Paslink and dynamic outdoor testing of building components, Building and Environment 43 (2) (2008) 143–151, special issue in outdoor testing analysis and modelling of building components, doi:10.1016/jbuildenv.2006.10.009.
[19] C. I. of Building Services Engineers, Environmental Design: CIBSE Guide A, CIBSE Guide, CIBSE, 2006.
[20] J.H. Watmuff, W.W.S. Charters, D. Proctor, Solar and Wind Induced External Coefficients – Solar Collectors, Tech. rep., 1977, June.
[21] C. Ghiaus, Causality issue in the heat balance method for calculating the design heating and cooling load, Energy 50 (2013) 292–301, http://dx.doi.org/10.1016/j.energy.2012.10.024.
[22] G. Oliveti, N. Arcuri, M.D. Simone, R. Bruno, Experimental evaluations of the building shell radiant exchange in clear sky conditions, Solar Energy 86 (6) (2012) 1785–1795, http://dx.doi.org/10.1016/j.solener.2012.03.009.
[23] J.A. Duffie, W.A. Beckman, Index, in Solar Engineering of Thermal Processes, Fourth Edition, John Wiley & Sons, Inc., Hoboken, NJ, USA, 2013, http://dx.doi.org/10.1002/9781118671603.index.
[24] Y. Tham, T. Muneer, Sol–air temperature and daylight illuminance profiles for the ukcp09 data sets, Building and Environment 46 (6) (2011) 1243–1250, http://dx.doi.org/10.1016/j.buildenv.2010.11.014.
[25] N.R. Kristensen, H. Madsen, S.B. Jrgensen, Parameter estimation in stochastic grey-box models, Automatica 40 (2) (2004) 225–237, http://dx.doi.org/10.1016/j.automatica.2003.10.001.
[26] N. Kristensen, H. Madsen, Continuous Time Stochastic Modelling CTSM 2.3 User Guide, 2003.
[27] N.R. Kristensen, H. Madsen, Continuous Time Stochastic Modelling, CTSM 2.3 – Mathematics Guide, Tech. rep., DTU, 2003.
[28] R. Juhl, ctsmr. CTSM for R, r Package Version 0.5.0-12, 2012.